The sedimentation rate of disordered suspensions

John F. Brady and Louis J. Durlofsky[a)]
Department of Chemical Engineering, California Institute of Technology, Pasadena, California 91125

(Received 2 November 1987; accepted 22 December 1987)

An explicit expression for the sedimentation velocity at low particle Reynolds number in a concentrated suspension is derived and evaluated for two different approximations to the hydrodynamic interactions: a strict pairwise additive approximation and a far-field, or Rotne–Prager, approximation. It is shown that the simple Rotne–Prager approximation gives a very accurate prediction for the sedimentation velocity of random suspensions from the dilute limit all the way up to close packing. The pairwise additive approximation, however, fails completely, predicting an aphysical negative sedimentation velocity above a volume fraction $\phi \approx 0.23$. The explanation for these different behaviors is shown to be linked to the "effective medium" behavior of the suspensions. It is shown analytically and by Stokesian dynamics simulation that a suspension of neutrally buoyant particles may be modeled as a homogeneous fluid with an effective viscosity, but a sedimenting suspension cannot. As a result, the Rotne–Prager approximation actually captures the correct features of the many-body interactions in sedimentation. An analytical expression for the sedimentation rate, which is in good agreement with experiment, is obtained using the Percus–Yevick hard-sphere distribution function.

I. INTRODUCTION

The rate at which particles suspended in a fluid medium settle under the force of gravity has yet to be determined theoretically in any general sense. The most basic problem, and the one that has received the greatest attention, is the sedimentation of a system of monodisperse spheres at very small particle Reynolds number. Even this problem, however, has only been solved for a limited range of conditions and only under fairly restrictive assumptions.

Many of the theoretical studies concerned with the sedimentation of monodisperse suspensions are reviewed by Davis and Acrivos[1]; we shall only mention a few of the most relevant. Batchelor[2] determined that the first correction to the nondimensionalized sedimentation velocity of a dilute, random suspension of monodisperse spheres is $O(\phi)$, where ϕ is the volume fraction of solids. This is to be contrasted with periodic systems, for which the first correction to the settling rate is $O(\phi^{1/3})$, considerably greater than for random systems.[3–6] These dilute suspension results are only applicable for $\phi < \sim 0.05$; much beyond this range they lose even qualitative accuracy. The $O(\phi)$ correction to the sedimentation velocity of random systems includes only pairwise hydrodynamic interactions. Extensions to higher order require that account be taken of many-body hydrodynamic interactions; this presents considerable difficulty. Reliable results for the sedimentation rate of concentrated suspensions are available, however, for periodic systems.[5,6] For these systems, the periodicity allows the solution of the many-body problem on the unit cell. In addition, as a result of the nature of the fundamental solution for periodic Stokes flow, convergence difficulties that arise for random systems are circumvented.

Glendinning and Russel,[7] applying a method developed by O'Brien,[8] derived a general expression for the sedimentation rate of a random suspension of spheres. In the Glendinning and Russel expression, which is not limited to low ϕ, a hard-sphere description of the suspension microstructure was used; that is, the distribution of particles was taken to be the same as that of a hard-sphere system at the same value of ϕ; particle interactions were, however, approximated in a strictly pairwise manner. At low ϕ, the resulting sedimentation velocities computed through this approach are in somewhat better agreement with experimental results than are the results of Batchelor. For $\phi > 0.27$, however, the predicted sedimentation velocity becomes negative, indicating the failure of the method for highly concentrated suspensions. This failure was attributed by Glendinning and Russel to the lack of many-body hydrodynamics in the approximation for particle interactions.

One possible way in which to incorporate many-body hydrodynamic interactions into suspension problems is to treat the suspension as an effective medium through which disturbances from a source particle propagate before being incident upon a test particle. One familiar example of such a medium is a Brinkman medium—a dilute suspension of particles fixed in space, where the many-body hydrodynamic interactions among the fixed particles change the fundamental nature of the medium. Specifically, disturbances far from a source point decay as $1/(\alpha^2 r^3)$, where α is a function of volume fraction and r is the distance. This is to be contrasted to the behavior in a pure fluid, where the interactions decay as $1/r$. Little is known, however, about the "effective" behavior of sedimenting systems. A related problem, about which considerably more is known, is the sedimentation of a single particle through a suspension of neutrally buoyant, or, equivalently, force-free particles. In this case, experimental and theoretical studies show that the suspension acts as a fluid, with an effective viscosity larger than that of the suspending fluid.[9,10] The fundamental nature of the disturbance caused by a point force is the same in this case as in a pure fluid; only the amplitude is affected by the presence of the

a) Present address: Chevron Oil Field Research Company, P.O. Box 446, La Habra, California 90633-0446.

 0031-9171/88/040717-11$01.90

neutrally buoyant particles. Not surprisingly, at low ϕ one may simply replace the fluid viscosity η by Einstein's viscosity $\eta(1+\frac{5}{2}\phi)$.

It is tempting to apply the effective medium behavior of a suspension of neutrally buoyant spheres to sedimenting systems; indeed this has been suggested.[7] The idea is that since the effective medium behavior is correct for a single falling particle, with the others neutrally buoyant, and since the Stokes equations are linear, we should be able to superimpose the effects of each individual particle. Despite this appealing notion, however, we shall see that the effective behavior of a suspension of neutrally buoyant spheres is not at all representative of the effective behavior of a sedimenting system; the superposition is not possible.

As shown by Beenakker and Mazur[10] and through an alternate method presented in the Appendix, it is the reflected stresslets, induced in the neutrally buoyant particles by the single sedimenting particle, that cause a suspension of neutrally buoyant particles to act as a fluid with an effective viscosity. (Recall that the stresslet is the symmetric part of the first moment of the force density integrated over the particle surface.) In sedimenting systems, however, the stresslet induced by one particle on a second particle is, as we shall see, effectively canceled by the stresslets induced on the second particle by third, fourth, etc., particles, negating the influence of the second particle on the motion of the first. Thus in sedimenting systems the medium may be approximated as one in which *no* stresslet interactions are present, i.e., *no* effective viscosity, in contrast to a suspension of neutrally buoyant particles. As we shall see, approximations that capture this aspect of interactions in sedimenting systems yield average sedimentation rates in good agreement with available empirical correlations.

In Sec. II we give a rigorous expression for the average sedimentation rate of a suspension and evaluate it for a hard-sphere microstructure. The sphere interactions are approximated in two ways: a strict pairwise approximation and a much more simple Rotne–Prager or far-field approximation, which includes no stresslet interactions. The Rotne–Prager approximation is seen to give results in much better agreement with experiment, suggesting that the lack of stresslet interactions is the key in understanding the effective behavior of sedimenting systems. In Sec. III we employ Stokesian dynamics,[11–13] a general molecular-dynamics-like method capable of simulating hydrodynamically interacting particles, to study stresslet interactions in both sedimenting systems and systems of neutrally buoyant particles. The qualitative differences between the two systems are clearly seen: Neutrally buoyant suspensions are shown to slow the sedimenting particle through induced stresslet interactions and the concept of an effective medium, specifically an effective viscosity, is seen to be valid. The stresslet interactions in sedimenting systems are shown, however, to have very little effect on the sedimentation rate; there is no effective medium behavior. This explains how the Rotne–Prager approximation, through its simplicity, actually incorporates the dominant many-body hydrodynamics in its description of particle–particle interactions and, as a result, provides an accurate estimate for the sedimentation rate.

The simplicity of the Rotne–Prager approximation allows us to develop in Sec. IV an analytical expression for the sedimentation rate—that is, a correlation based on the physics of particle interactions—that may find use in other studies of sedimenting systems.

II. AVERAGE SEDIMENTATION RATE OF A HARD-SPHERE SUSPENSION

In this section we shall derive an expression for determining the average sedimentation rate of a suspension. Evaluation of this expression will require information on the distribution of particles and an approximation for particle–particle interactions in sedimenting systems. Results for the sedimentation rate will be presented for a hard-sphere microstructure using two different approximations for the sphere–sphere interactions. We now proceed with the derivation of the formal expression for the average sedimentation rate.

The derivation follows the method of O'Brien[8] for constructing convergent expressions for particle interactions in suspensions. This is the same method employed by Glendinning and Russel,[7] although our final result differs somewhat from their result. (The difference is not important for the material to be discussed in this paper.) Since a detailed derivation of the convergent expression can be found in Brady *et al.*,[13] here we shall only sketch the development.

We start with the integral representation for the solution to the Stokes equations for the velocity field $\mathbf{u}(\mathbf{x})$ at any point $\mathbf{x}$ in the fluid in terms of integrals of the force distribution on the surfaces of the particles and an intergral over a mathematical surface Γ' of large radius lying entirely within the fluid:

$$u_i(\mathbf{x}) = -\frac{1}{8\pi\eta}\sum_{\alpha=1}^{N}\int_{S_\alpha} J_{ij}(\mathbf{x}-\mathbf{y})\sigma_{jk}(\mathbf{y})n_k(\mathbf{y})dS_y - \frac{1}{8\pi\eta}\int_{S_{\Gamma'}}[J_{ij}(\mathbf{x}-\mathbf{y})\sigma_{jk}(\mathbf{y}) + 2\eta K_{ijk}(\mathbf{x}-\mathbf{y})u_j(\mathbf{y})]n_k(\mathbf{y})dS_y. \quad (1)$$

Here, J_{ij} is the Green's function for the Stokes flow

$$J_{ij}(\mathbf{r}) = \delta_{ij}/r + r_i r_j/r^3 \quad (2)$$

and

$$K_{ijk}(\mathbf{r}) = -3r_i r_j r_k/r^5. \quad (3)$$

We define δ_{ij} as the unit isotropic tensor, η as the viscosity of the suspending fluid, and σ as the fluid stress tensor:

$$\sigma_{ij} = -p\delta_{ij} + 2\eta e_{ij}, \quad (4)$$

where p is the pressure and $e_{ij} = \frac{1}{2}(\nabla_i u_j + \nabla_j u_i)$ is the rate of strain tensor. We note that $\mathbf{r} = \mathbf{x} - \mathbf{y}$, with $\mathbf{y}$ a point on the surface and n the outer normal to the surfaces, i.e., pointing into the volume V containing the N particles.

Equation (1) is an exact formulation for rigid particles. (Recall that for rigid particles $\int_{S_\alpha} K_{ijk}u_j n_k\, dS = 0$.) No divergences occur because we have a finite region bounded by the surface Γ'. This is an arbitrary surface immersed in an unbounded statistically homogeneous suspension, i.e., the suspension continues outside of Γ'. If the radius R of this

surface is taken to be very large (with the origin located near the field point $\mathbf{x}$), the variation in $\mathbf{J}$ and $\mathbf{K}$ will be small over a surface element $dS_{\Gamma'}$ that passes through the fluid and around many particles. Thus in the integrand of the second integral we may replace σ and $\mathbf{u}$ by averages. This is facilitated by first transforming from Γ' to a smooth macroscopic surface Γ that cuts both the fluid *and* particles; the averages thus formed are *suspension averages*—fluid and particle phase averages. Following a procedure similar to that used by Glendinning and Russel, it may be shown that[13]

$$\int_{S_{\Gamma'}} (J_{ij}\sigma_{jk} + 2\eta K_{ijk}u_j)n_k \, dS_y$$
$$= \int_{S_\Gamma} (J_{ij}\langle\sigma_{jk}\rangle n_k + 2\eta K_{ijk}\langle u_j\rangle n_k$$
$$- n\nabla_k J_{ij}\langle Q'_{klj}\rangle n_l) dS_y. \tag{5}$$

Here, $\langle\sigma\rangle$ and $\langle\mathbf{u}\rangle$ are the suspension average hydrodynamic stress and velocity and $\langle\mathbf{Q}'\rangle$ is the average quadrupole density of the particles. The quadrupole of the particle α is defined by

$$Q'^{\alpha}_{klj} \equiv -\frac{1}{2}\int_{S_\alpha} (y_k - x^\alpha_k)(y_l - x^\alpha_l)\sigma_{jm}n_m \, dS_y, \tag{6}$$

where $\mathbf{x}^\alpha$ is the "center" of particle α. The derivative of $\mathbf{J}$ in the quadrupole integral is with respect to $\mathbf{y}$ and $n = N/V$ is the number density of the particles.

The use of the suspension average quantities is the key step and the *only* assumption made in O'Brien's method. In a statistically homogeneous medium $\langle\sigma\rangle$ and $\langle\mathbf{u}\rangle$ are either constants or linear functions of position, coming from the average pressure in $\langle\sigma\rangle$ and a linear shear flow in $\langle\mathbf{u}\rangle$, while $\langle\mathbf{Q}'\rangle$ is constant. With Eq. (5), Eq. (1) becomes

$$u_i(\mathbf{x}) = -\frac{1}{8\pi\eta}\sum_{\alpha=1}^{N}\int_{S_\alpha} J_{ij}\sigma_{jk}n_k \, dS_y$$
$$-\frac{1}{8\pi\eta}\int_{S_\Gamma} (J_{ij}\langle\sigma_{jk}\rangle n_k + 2\eta K_{ijk}\langle u_j\rangle n_k$$
$$- n\nabla_k J_{ij}\langle Q'_{klj}\rangle n_l) dS_y. \tag{7}$$

In the sum over α, only the particle surfaces that lie within Γ are included.

Equation (7) is the key result of O'Brien's method and leads to convergent expressions for the fluid velocity at any point $\mathbf{x}$, as well as for the hydrodynamic interactions among the particles. By use of the divergence theorem, the macroscopic boundary integral over Γ can be converted into a volume integral of uniform distributions of average forces (monopoles), dipoles, and quadrupoles. At large distances from the field point $\mathbf{x}$, we may expand the force density on the surface of a particle α in moments; the sum over α in Eq. (7) will approximate a volume integral of a continuous distribution of average monopoles, dipoles, and quadrupoles. Thus the sum and integral will cancel, leaving a finite result for the velocity. Note that the velocity disturbance caused by a quadrupole decays as $1/r^3$, while the next moment in the expansion of the particle surface force density, the octupole, creates a disturbance that decays as $1/r^4$; thus the sum over the octupoles and higher moments is absolutely convergent. This is the essence of the method.

Using the divergence theorem and Faxén laws for particle velocities, Eq. (7) can be used to derive the following equation for the translational velocity of an arbitrary spherical particle, which we label α:

$$U^\alpha_i - \langle u_i(\mathbf{x}^\alpha)\rangle$$
$$= \left(\phi - \frac{1}{5}\phi^2\right)\frac{\langle F_i\rangle}{6\pi\eta a} + \frac{F^\alpha_i}{6\pi\eta a}$$
$$- \frac{1}{8\pi\eta}\sum_{\beta\neq\alpha}\int_{S_\beta}\left(1 + \frac{a^2}{6}\nabla^2\right)J_{ij}\sigma_{jk}n_k \, dS$$
$$- \frac{n}{8\pi\eta}\int_V\left[1 + \frac{a^2}{3}\left(1 - \frac{1}{5}\phi\right)\nabla^2\right]J_{ij}\langle F_j\rangle dV. \tag{8}$$

Here, $\langle\mathbf{u}(\mathbf{x}^\alpha)\rangle$ is the suspension average velocity evaluated at the center of particle α; $\mathbf{F}^\alpha$ is the force the αth particle exerts on the fluid, i.e., $F^\alpha_i = -\int_{S_\alpha}\sigma_{jk}n_k \, dS$; and $\langle\mathbf{F}\rangle = (1/N)\sum_{\alpha=1}^{N}\mathbf{F}^\alpha$ is the average force all the particles exert on the fluid. In obtaining Eq. (8) we have made use of the fact that the average torque and the stresslet in a sedimenting suspension are zero. We have also used a mean-field approximation for the particle quadrupoles [cf. Eqs. (2.23) and (2.29) of Brady *et al.*[13]], resulting in the $\phi^2\langle\mathbf{F}\rangle$ and the $\phi\nabla^2$ terms in the volume integral.

If we average Eq. (8) over the positions of all possible particles β and over all particles α, we obtain for the *average* sedimentation velocity,

$$\langle\mathbf{U}\rangle - \langle\mathbf{u}\rangle$$
$$= \left(1 - 5\phi - \frac{1}{5}\phi^2\right)\langle\mathbf{F}\rangle + \phi\frac{9}{16\pi}\int_2^\infty\left\{P_{1/1}(\mathbf{r}|\mathbf{0})\right.$$
$$\times\left[-\int_{S_y}\left(1 + \frac{1}{6}\nabla^2\right)\mathbf{J}\cdot\langle\sigma\rangle_1\cdot\mathbf{n} \, dS\right]$$
$$\left.-\left[1 + \frac{1}{3}\left(1 - \frac{1}{5}\phi\right)\nabla^2\right]\mathbf{J}\cdot\langle\mathbf{F}\rangle\right\}dV. \tag{9}$$

Here, $P_{1/1}(\mathbf{r}|\mathbf{0})$ is the conditional probability density, normalized by n, for finding a particle at position $\mathbf{r}$ given that there is a particle at the origin $\mathbf{0}$. We note that $\langle\sigma(\mathbf{y}|\mathbf{0})\rangle_1$ is the average stress at the point $\mathbf{y}$ on the surface of the particle whose center is at $\mathbf{r}$, conditioned on the presence of a particle at $\mathbf{0}$. All lengths have been nondimensionalized by the sphere radius and the force has been nondimensionalized by $6\pi\eta a U_0$, where U_0 is the Stokes settling velocity of an isolated particle. The velocities have been nondimensionalized by U_0. The lower limit of integration is at $r = 2$, corresponding to the fact that $P_{1/1} = 0$ for $r < 2$ for impenetrable spheres.

In order to determine the average sedimentation velocity relative to the suspension average velocity $\langle\mathbf{u}\rangle$, which we shall take to be zero, we need two different pieces of information. We need some knowledge of the distribution of particles through the conditional probability $P_{1/1}$, and we need some approximation (or exact expression) for the conditionally averaged force density $\langle\sigma\rangle_1$ on the particle surface. We shall treat these two aspects in turn, but it may help the reader to note that if we approximate $\langle\sigma\rangle_1$ by the stress distribution that would exist if there were only two particles in the system (one particle at $\mathbf{r}$ and the other at $\mathbf{0}$), then, in the limit $\phi\to 0$, Eq. (9) reduces to the expression of Batchelor. The sedimentation velocity $\langle\mathbf{U}\rangle - \langle\mathbf{u}\rangle = (1 - 6.55\phi)\langle\mathbf{F}\rangle$

for an isotropic, homogeneous random suspension with $P_{1/1} = 1$.

The conditional probability density $P_{1/1}$ is generally known as the pair-distribution function. In the absence of any other information, we shall assume that the suspension microstructure is described by a hard-sphere structure at the same value of ϕ. Then $P_{1/1}(\mathbf{r}|\mathbf{0})$ is isotropic and equal to $g(r;\phi)$, the radial-distribution function for a hard-sphere system, where we have shown explicitly that g depends parametrically on ϕ. This would be the correct microstructure in the limit of strong Brownian motion and represents a convenient reference state. If other information is available on $P_{1/1}$, it could be used directly in Eq. (9).

The hard-sphere radial-distribution function can be approximated in a variety of ways, most notably through the use of the Percus–Yevick equation or by Monte Carlo simulation. Because analytic solutions to the Percus–Yevick equation are available,[14–17] it is desirable to use this description. At high volume fractions, however, the Percus–Yevick $g(r)$ loses accuracy, deviating noticeably from Monte Carlo results,[18] which are considered to provide the most accurate approximation to the hard-sphere radial-distribution function. To address this difficulty, Verlet and Weis[19] devised a largely empirical adjustment to the Percus–Yevick $g(r)$, which brings it into excellent agreement with Monte Carlo results. Using the expressions given by Smith and Henderson[17] for the Percus–Yevick $g(r)$ in conjunction with the procedure of Verlet and Weis,[19] we have a very accurate approximation $g(r)$. At large values of r ($r > 10$ sphere radii), however, the exact Percus–Yevick solution becomes exceedingly complex; in this range of r, therefore, we use the far-field form of $g(r)$, given by Perry and Throop,[20] with the coefficients determined through a fit of the $9.5 < r < 10$ $g(r)$ results. Shown in Fig. 1 are hard-sphere $g(r)$ results for a dense system ($\phi = 0.4712$) computed through the Percus–Yevick equation[16] (dashed line), by Monte Carlo simulation[18] ($\times$'s), and through the adjusted Percus–Yevick procedure (solid line), as described above. The excellent agreement between the Monte Carlo and adjusted Percus–Yevick results is apparent, as is the deviation of the Percus–Yevick result in the range $2 \leqslant r \leqslant 2.5$.

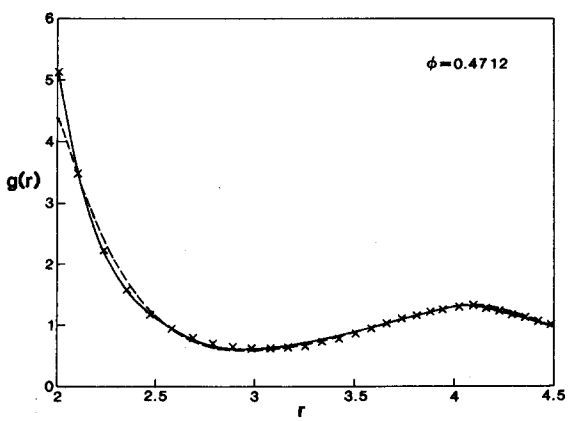

FIG. 1. The hard-sphere radial distribution function at $\phi = 0.4712$ computed via Monte Carlo simulation[18] ($\times$), the Percus–Yevick equation[16] (- - -), and the adjusted Percus–Yevick equation (—). Note the excellent agreement between the Monte Carlo results, considered exact, and the adjusted Percus–Yevick equation.

The only issue left to address before evaluating Eq. (9) for various values of ϕ is how to approximate $\langle\sigma\rangle_1$, i.e., how to approximate the hydrodynamic interaction between the particle at $\mathbf{r}$ and the test particle at $\mathbf{0}$ *in* the suspension. We shall approximate this interaction in two ways. The first is a strictly pairwise additive approximation, which assumes that the two spheres in suspension interact exactly as they would if they were alone in the fluid. In this case, $\langle\sigma\rangle_1$ can be found by solving a two-sphere problem and the interactions in Eq. (9) can be expressed in terms of the two-sphere mobility functions, as given by Jeffrey and Onishi.[21] Rewriting Eq. (9) in terms of mobility functions and noting that for an isotropic suspension $\langle\mathbf{U}\rangle$ is parallel to $\langle\mathbf{F}\rangle$, we have

$$\langle U\rangle - \langle u\rangle = 1 - 5\phi - \frac{1}{5}\phi^2 + \phi\int_2^\infty g(r)\left[x_{11}^a + x_{12}^a + 2(y_{11}^a + y_{12}^a) - 3\left(1 + \frac{1}{r}\right)\right] r^2\,dr + 3\phi\int_2^\infty [g(r) - 1]r\,dr, \tag{10}$$

where the mobility functions x_{11}^a, x_{12}^a, etc., follow the notation of Jeffrey and Onishi.[21] We should note that Eq. (10) also applies if we do not assume pairwise additivity. In this case, the mobility functions are the two-sphere interactions in the dense suspension.

The second approximation we shall make is to assume that the only interaction between the two particles is a far-field Rotne–Prager interaction, that is, the far-field part of the interaction between two particles alone in the fluid. The Rotne–Prager approximation neglects any induced interactions between the particles and simply says that the translational velocity of the test particle due to the second particle is just the velocity disturbance caused by the second particle alone in the fluid. Thus the translational velocity of the test particle is approximated to $O(1/r^3)$, where r is the spacing between the two particles. In terms of the mobility functions appearing in Eq. (10), the Rotne–Prager approximation is given by

$$\begin{aligned} x_{11}^a &= 1, \quad x_{12}^a = \tfrac{3}{2}r^{-1} - r^{-3}, \\ y_{11}^a &= 1, \quad y_{12}^a = \tfrac{3}{4}r^{-1} + \tfrac{1}{2}r^{-3}. \end{aligned} \tag{11}$$

Note that introducing these functions into Eq. (10) causes the first integral on the right-hand side to vanish.

In contrast to the Rotne–Prager approximation given by Eq. (11), the strict pairwise additive approximation includes effects to all orders in $1/r$. Despite its greater complexity, the strict pairwise additive approximation ignores all third- and higher-body effects. While at first it may seem that the Rotne–Prager approximation also ignores all third- and higher-body effects, as we shall see below, this approximation actually does incorporate the dominant many-body effects and therefore gives a better estimate of the average sedimentation rate.

Evaluating $g(r)$ as described above, the integrations in Eq. (10) were performed using Simpson's rule with a very fine discretization (5000–9000 points) for the two different approximations for the mobility functions. At low and mod-

erate values of ϕ ($\phi \leqslant 0.38$) the integrations were carried out for $2 \leqslant r \leqslant 10$; for larger values of ϕ the range of r was $2 \leqslant r \leqslant 16$. In both cases further discretization or extension of the upper limit of integration had no effect on the results.

Shown in Fig. 2 is the average sedimentation rate as a function of ϕ. The circles correspond to the first approximation, i.e., the strict pairwise additive approximation and the $\times$'s correspond to the Rotne–Prager approximation. The $+$ symbols correspond to a third approximation and the dashed line is an analytical result, both of which are discussed in Sec. IV. The solid line is a correlation of the experimental data given in Ref. 22. Clearly, the results with the two-sphere interactions approximated via the Rotne–Prager tensors are in much better agreement with the empirical results than are those with the strict pairwise additive approximation. In fact, the strict pairwise additive result predicts negative sedimentation velocities, an obviously aphysical result, for $\phi > 0.23$. From Fig. 2 it seems as though the Rotne–Prager tensor provides the better description of two-sphere interactions in a sedimenting suspension.

Before considering why this might be the case, let us digress to consider the closely related problem of the motion of a single particle sedimenting through a suspension of neutrally buoyant particles. In this case, as discussed in Sec. I, experiments indicate that the suspension of neutrally buoyant particles acts as a fluid with an effective viscosity larger than that of the suspending fluid.[9] In fact, at low ϕ, the effective viscosity of the suspension η_{eff} is precisely the Einstein viscosity $(1 + \frac{5}{2}\phi)\eta$. Beenakker and Mazur[10] showed this effect to be caused by the reflections of stresslets induced on the neutrally buoyant particles by the sedimenting particle. An alternative development yielding the same result is presented in the Appendix. The interaction between the sedimenting particle and a single neutrally buoyant particle a distance r away is as follows: The sedimenting particle propagates a point force disturbance decaying as $1/r$ (for our purposes here, the sedimenting particle can be considered a point force), which induces a stresslet of magnitude $O(1/r^2)$ in the neutrally buoyant particle. The neutrally buoyant particle in turn propagates a velocity field of $O(1/r^2)$ times the stresslet intensity, resulting in an $O(1/r^4)$ velocity disturbance, which *opposes* the motion of the sedimenting particle. To a first approximation, each neutrally buoyant particle behaves in this way and integrating over all neutrally buoyant particles results in the "effective" behavior of the suspension (cf. the Appendix). The key point in the above discussion is that the sedimenting particle induces stresslets in the neutrally buoyant particles, which causes them to propagate velocity fields opposed to the motion of the sedimenting particle.

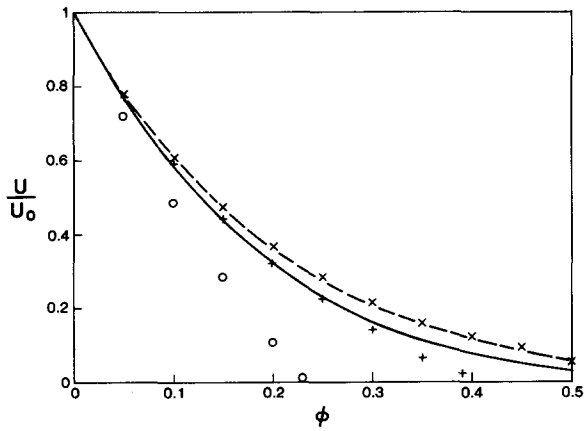

FIG. 2. The dimensionless average sedimentation rate of a disordered system of monodisperse spheres as a function of volume fraction. The $\times$'s correspond to the theoretical result [Eq. (9)] with the sphere–sphere interactions approximation via the Rotne–Prager approximation; the O's correspond to the strict pairwise additive approximation for sphere–sphere interactions; the $+$'s correspond to the stresslet-free approximation for sphere interactions (discussed in Sec. IV); — is an empirical result[22]; and - - - is an analytical expression [Eq. (16)] for the Rotne–Prager approximation with the Percus–Yevick hard-sphere distribution. The strict pairwise approximation predicts negative sedimentation velocities for $\phi > 0.23$ and the stresslet-free approximation for $\phi > 0.39$.

The effective behavior of the free suspensions described above would *not* be captured if sphere interactions were approximated via the Rotne–Prager tensor, which does not include any induced stresslet interactions. By contrast, the strict pairwise approximation would describe the effective medium behavior of a suspension of neutrally buoyant spheres to a first approximation. This might at first seem in conflict with the results displayed in Fig. 2, where the Rotne–Prager description of spheres in a sedimenting suspension is clearly superior. There is, however, a rather simple way in which to understand the effects of induced stresslets and therefore the effective medium, and why the Rotne–Prager approximation works so well.

The basic problem is the approximation of the conditionally averaged stress, $\langle \sigma(\mathbf{r}|\mathbf{0}) \rangle_1$, on the surface of the particle at $\mathbf{r}$ in Eq. (9). If we expand this force density in moments, the zeroth moment, or monopole, is the total force $\langle \mathbf{F}(\mathbf{r}|\mathbf{0}) \rangle_1$, which equals the average force $\langle \mathbf{F} \rangle$ since all particles have the same prescribed force. The first moment, or dipole, has antisymmetric and symmetric parts, which are the torque $\langle \mathbf{L}(\mathbf{r}|\mathbf{0}) \rangle_1$ and stresslet $\langle \mathbf{S}(\mathbf{r}|\mathbf{0}) \rangle_1$, respectively. For sedimentation the torque on each particle is zero and therefore the first effect of particle interactions is through the conditionally averaged stresslet $\langle \mathbf{S}(\mathbf{r}|\mathbf{0}) \rangle_1$. In the strict pairwise additive calculation, we approximate the conditionally averaged stresslet as the stresslet of the particle at $\mathbf{r}$ due to the particle at $\mathbf{0}$ when the two particles are alone in the fluid. In the Rotne–Prager calculation we approximate the conditionally averaged stresslet with the *suspension* average stresslet, which is zero in a statistically homogeneous medium. (The fact that the average stresslet must be zero can easily be seen by noting that the only vector in the problem is the gravitational force $\langle \mathbf{F} \rangle$; there is no way to construct a second-order tensor linear in $\langle \mathbf{F} \rangle$ in an isotropic medium.) The Rotne–Prager approximation is actually a better representation of the behavior in concentrated suspension and therefore provides a better estimation of the sedimentation rate.

From the above discussion it seems as though the stresslet interactions are the key to understanding the difference between free and sedimenting suspensions. These interactions can best be studied through simulation, as described in Sec. III, where we shall show that the conditionally averaged stresslet and its effect on the sedimentation velocity are indeed small and well approximated by zero.

III. STRESSLETS IN SEDIMENTING AND FREE SUSPENSIONS

The general Stokesian dynamics simulation method is presented in detail elsewhere.[11–13] Here, we shall very briefly review the method and discuss its application to the problem at hand. The specific issues we wish to address are (i) how do the stresslet intensities of particles in suspension differ when one versus all sediment and, more important, (ii) how do the stresslet intensities affect particle velocities in the two cases?

Consider a system of N spheres in a volume V replicated periodically throughout all space. At zero-particle Reynolds number a far-field approximation to the N-sphere grand mobility matrix $\mathscr{M}^*$ can be formed through a moment expansion of the integral solution for the Stokes flow and the application of the Faxén laws. The resulting equation set is

$$\begin{pmatrix} \mathbf{U} - \langle \mathbf{u} \rangle \\ -\mathbf{E} \end{pmatrix} = \begin{pmatrix} \mathbf{M}^*_{UF} & \mathbf{M}^*_{US} \\ \mathbf{M}^*_{EF} & \mathbf{M}^*_{ES} \end{pmatrix} \cdot \begin{pmatrix} \mathbf{F} \\ \mathbf{S} \end{pmatrix}, \tag{12}$$

where $\mathbf{U}$ is the particle translational/rotational velocity vector, $\langle \mathbf{u} \rangle$ is the suspension average translational/rotational velocity vector, $\mathbf{E}$ is the suspension average rate of strain, and $\mathbf{F}$ specifies the force/torque and $\mathbf{S}$ the stresslet exerted by each particle on the fluid. The submatrices $\mathbf{M}^*_{UF}$, $\mathbf{M}^*_{US}$, $\mathbf{M}^*_{EF}$, and $\mathbf{M}^*_{ES}$ comprise $\mathscr{M}^*$; note that their subscripts indicate the kinematic and dynamic quantities they relate. The asterisks indicate that the matrices are formed with the application of the Ewald summation technique (see Ref. 13 for details), which assures that interactions among all particles and all their images in other periodic cells are included in the simulation. In the present problem, the far-field approximation to $\mathscr{M}^*$ will suffice to illustrate the qualitative effects we seek. Thus the effort expended in other simulation studies to include near-field lubrication interactions is not required here.

Equation (12) can be solved for $\mathbf{S}$ in terms of $\mathbf{E}$ and $\mathbf{F}$. In the case $\mathbf{E} = 0$, i.e., no imposed shear flow, we have

$$\mathbf{S} = -(\mathbf{M}^*_{ES})^{-1} : \mathbf{M}^*_{EF} \cdot \mathbf{F}, \tag{13}$$

while for the particle velocities we have

$$\mathbf{U} - \langle \mathbf{u} \rangle = \mathbf{M}^*_{UF} \cdot \mathbf{F} + \mathbf{M}^*_{US} : \mathbf{S}. \tag{14}$$

We identify the $\mathbf{M}^*_{US}:\mathbf{S}$ term on the rhs of Eq. (14) as $\mathbf{U}^S$, the velocity due to the induced stresslets: It is this term, the contribution to the sedimentation velocity from the stresslets, in which we are most interested.

The simulations are performed for systems of spheres confined to a plane. Such monolayer simulations are useful because the number of degrees of freedom of the system is reduced, specifically from 11 to 6, resulting in computational savings, while the essential physics is maintained. The density measure in monolayer systems is the areal fraction ϕ_A, given by

$$\phi_A = N\pi a^2 / H^2, \tag{15}$$

where H is the length of a side of the periodic cell, assumed square. At a given value of the areal fraction, several disordered configurations of spheres are generated via a Monte Carlo technique. These disordered configurations of spheres confined to a plane should describe a hard-disk radial-distribution function; this is in fact verified through comparison with available hard-disk $g(r)$ results.[23] Given these disordered configurations of spheres in a monolayer, $\mathbf{M}^*_{ES}$ and $\mathbf{M}^*_{EF}$ [note that $\mathbf{M}^*_{US} = (\mathbf{M}^*_{EF})^\dagger$] are formed. By prescribing $\mathbf{F}$ in Eq. (13), $\mathbf{S}$ is calculated for the case of one sphere sedimenting with the others force-free and for the case of all sedimenting. Note that the prescribed force lies in the plane of the monolayer. Given $\mathbf{S}$, the velocity due to the induced stresslets, $\mathbf{U}^S$, can be calculated for the two cases. By averaging over all the spheres in the system and by performing multiple realization (typically three), a large body of statistics is generated. In all the simulation results presented, $N = 121$.

Shown in Fig. 3 are simulation results for $-U^S_x$ as a function ϕ_A, where U^S_x is the component of $\mathbf{U}^S$ in the direction of the imposed force. The $\times$'s, corresponding to one particle sedimenting, show a clear increase in $-U^S_x$ with ϕ_A, while the circles, corresponding to all particles sedimenting, deviate very little from zero for all values of ϕ_A and show little discernible trend. Thus we conclude from the simulation results that when one sphere sediments and the rest are neutrally buoyant, the neutrally buoyant spheres act, through their induced stresslets, as an effective viscous medium and slow the sedimenting sphere as expected. By contrast, when all sediment, there is little to no effect on the sedimentation velocity from induced stresslets. At low ϕ_A ($\phi_A = 0.1$), however, the averages for the two cases are nearly the same, indicating that they behave similarly as $\phi_A \to 0$. This point will be discussed in greater detail in Sec. IV.

Standard deviations for $-U^S_x$ are not shown in Fig. 3, although their magnitudes are of some interest. For the case of one sphere sedimenting with the rest neutrally buoyant, the standard deviation in $-U^S_x$ varies relatively little with ϕ_A, ranging from a minimum of 0.025 at $\phi_A = 0.1$ to a maximum of 0.034 at $\phi_A = 0.5$. When all spheres sediment, however, the standard deviation increases with increasing ϕ_A from 0.029 at $\phi_A = 0.1$ to 0.097 at $\phi_A = 0.6$. In computing these standard deviations, each sphere in each realization is considered independent.

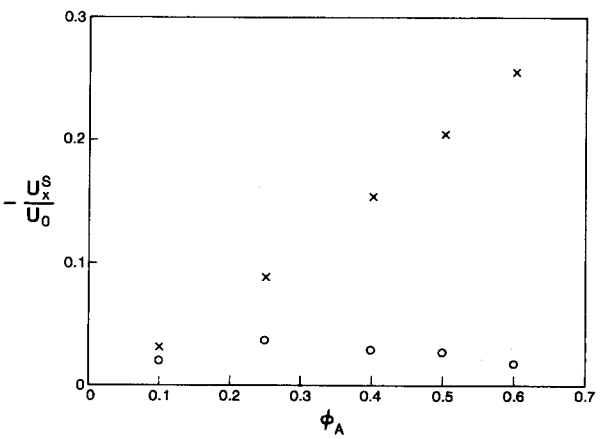

FIG. 3. The dimensionless contribution to the sedimentation rate from induced stresslets as a function of areal fraction. The $\times$'s correspond to simulation results for which one sphere sediments and the others are neutrally buoyant and the O's correspond to simulation results for which all sediment. When all spheres sediment, the induced stresslets have little effect on the sedimentation rate.

The results presented in Fig. 3 indicate that induced stresslets have little effect on the sedimentation rate of hard-sphere suspensions. This is also the situation for sedimenting periodic systems. In the periodic case, the stresslets on all spheres are identically zero, resulting in $U_x^S = 0$ for all ϕ_A. Because of the regular arrangement of particles in a periodic lattice, the stresslet induced by a sphere α on a sphere β is *exactly* canceled by the stresslet induced on sphere β by a third sphere γ. Exact cancellation does not occur in disordered systems; rather, the stresslets cancel on average over a small element of volume and thus their net effect on the sedimentation velocity is essentially zero.

This is illustrated in Figs. 4(a) and 4(b), where the xy component of the stresslet, S_{xy}, is plotted versus θ at particular values of r ($r = 2.40$ and 7.15) for simulations at $\phi_A = 0.4$ in which the imposed force is in the x direction. Results are shown for both the cases of one (solid lines) and all (dashed lines) spheres sedimenting. For the case of one particle sedimenting, the results are determined by discretizing space in r and θ about the sedimenting sphere [see Fig. 4(a) for the coordinate system] and averaging the induced stresslets of all spheres within a area element $r\Delta r\Delta\theta$. This averaging process is extended by considering each sphere in turn as the sedimenting sphere. For the case of all spheres sedimenting, the averaging proceeds as above, with each sphere in turn considered as the central sphere, relative to which the averages are computed. Further, the results shown in Figs. 4(a) and 4(b) are averages over six realizations; the vertical lines indicate the θ-average standard deviations between the six realizations. It is apparent from Fig. 4(a) that S_{xy} displays a statistically significant variation with θ at $r = 2.40$ in both the case when one sphere sediments and when all sediment. When all sediment, however, this variation is slight and the standard deviation between the six realizations is relatively large. For $r > 4$, S_{xy} no longer displays a statistically significant variation with θ when all spheres sediment (i.e., S_{xy} is essentially zero), although it continues to vary significantly with θ and in the same way as in Fig. 4(a), at all values of r when only one sphere sediments. These observations are clearly illustrated in Fig. 4(b). Note the extremely large standard deviation between the six realizations in the case when all spheres sediment, indicating that the θ variation is not significant.

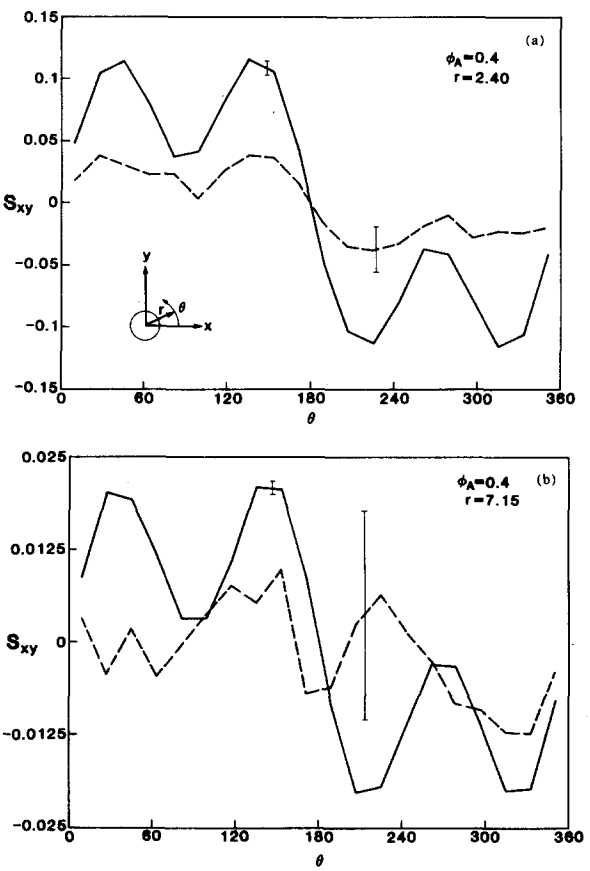

FIG. 4. Simulation results for the xy component of the stresslet as a function of angle θ [defined in (a)] for spheres a distance (a) $r = 2.40$ and (b) $r = 7.15$ away from central sphere for $\phi_A = 0.4$. The solid lines (—) correspond to the case of the central sphere sedimenting with the rest neutrally buoyant and the dashed lines (- - -) correspond to the case of all sedimenting. The vertical lines indicate standard deviations over six realizations. The S_{xy} result for all spheres sedimenting in (a) displays a statistically significant variation with θ; in (b) there is no statistically significant variation.

Thus the qualitative explanation for the difference between the U_x^S results in the case of one versus all spheres sedimenting is the following: When all spheres sediment, the stresslet induced by a sphere α on a sphere β is essentially negated (on average) by the stresslets induced by other sedimenting spheres located near sphere β. Although there is some local structure with the stresslet of β depending on α, quite rapidly this correlation is lost; as a result U_x^S is nearly zero. When only one sphere sediments, however, other sedimenting spheres are not present to negate the effect of the stresslet induced on sphere β, the correlation persists for all r, and U_x^S is nonzero. Thus the simple notion of an effective viscosity is correct when a single particle is sedimenting (coming from the correlated stresslets), but it is not applicable to the case when all particles are sedimenting, with the possible exception of $\phi \to 0$, as discussed below.

We now see quite clearly why the Rotne–Prager tensor provides a better approximation of the interactions of sedimenting spheres than does the full, pure fluid two-sphere interaction. As discussed at the end of Sec. II, the Rotne–Prager tensor does not include induced stresslet interactions, or any other higher moments for that matter, in its description of two-sphere interactions. In using the Rotne–Prager interaction in Eq. (9), therefore, we have implicitly set all higher moments to zero. By contrast, the full two-sphere interaction includes induced stresslets (and higher moments) and their effect on the average sedimentation rate. Because these interactions are included when they should not be present, the sedimentation velocity decreases faster with ϕ than it should and the resulting average sedimentation rate becomes negative for $\phi > 0.23$.

IV. DISCUSSION

From the results presented in Secs. II and III it is clear that the Rotne–Prager approximation yields reasonable results for the average sedimentation rate at least in part because it neglects induced stresslet interactions. However, it must be emphasized that the Rotne–Prager approximation neglects all higher moments in the expansion of $\langle\sigma\rangle_1$ as well.

Therefore, it is of interest to investigate other approximations for two-sphere interactions that neglect stresslet interactions, but include higher moments, in an effort to understand the effects of higher moments in sedimenting systems.

One way the effects of higher moments can be studied is through application of the exact two-sphere resistance formulation of Kim and Mifflin.[24] By writing the two-sphere resistance matrix in a form analogous to Eq. (12) and requiring the stresslets to be zero (note that this entails E to be nonzero), a matrix relating U and F is formulated. From this "stresslet-free" mobility matrix, the scalar functions x_{11}^a, x_{12}^a, etc., are determined. These scalar functions contain all moments with the exception of the stresslet. By introducing these stresslet-free mobility functions into Eq. (10), we can assess the effect of the higher moments of sphere interactions in sedimenting systems.

The results of this calculation are shown as the + symbols in Fig. 2. From Fig. 2 it is clear that the stresslet-free mobility interactions result in average sedimentation rates that agree well with the empirical result (solid line) for $\phi \leqslant 0.3$, but for $\phi > 0.39$ the sedimentation velocities become negative, indicating that the stresslet-free mobility interactions lose validity for large ϕ. Thus, at least at large ϕ, differences between the sedimentation rates predicted with the Rotne–Prager approximation and the stresslet-free mobility interactions are evident, indicating that the effects of the higher moments of sphere interactions in sedimenting systems are of some importance.

In the moment expansion of the integral solution of the Stokes flow, the moments following the stresslet are the quadrupole, octupole, hexadecupole, etc., propagating velocity fields of $O(1/r^3)$, $O(1/r^4)$, $O(1/r^5)$, etc. Portions of these moments are reducible, i.e., they can be expressed in terms of lower moments. For example, part of the quadrupole can be expressed in terms of the force and gives rise to the $(a^2/6)\nabla^2$ term in the Faxén law. The portions of the higher moments that cannot be expressed in terms of lower moments are referred to as irreducible. Proceeding from a moment expansion point of view, the first-order approximation to sphere interactions in sedimenting systems is the Rotne–Prager approximation, which incudes force and reducible quadrupolar interactions. The next moment is the stresslet, which we have seen to be essentially zero in sedimenting systems and can therefore be neglected. Thus, the first correction to the Rotne–Prager tensor arises from irreducible quadrupole interactions. Because this portion of the quadrupole is induced, it is $O(1/r^6)$. Note that we have already included the mean-field irreducible quadrupole contribution, giving the constant $-\frac{1}{5}\phi^2$ term in Eq. (9); thus the first correction to the Rotne–Prager approximation is $O(1/r^6)$. The next moment, the octupole, can be expected to be essentially zero in sedimenting systems, just as was the stresslet. This is because both the stresslet and octupole are odd moments of the force density and the cancellation seen to occur with stresslets will also occur for all odd moments. Thus there is no $O(1/r^8)$ contribution.

The Rotne–Prager approximation neglects terms of $O(1/r^6)$, while the stresslet-free mobility functions are in error at $O(1/r^8)$ through their inclusion of octupoles, which should be neglected. Therefore, because of a seemingly smaller error, it might be expected that the stresslet-free mobility functions would better approximate sphere interactions in sedimenting systems. Judging from Fig. 2, however, this is not the case. We can only speculate that either the $O(1/r^6)$ terms neglected in the Rotne–Prager approximation have small coefficients, while the $O(1/r^8)$ terms incorrectly included in the stresslet-free mobility functions have large coefficients, or that there are some compensating errors in the Rotne–Prager approximation. For example, it may be that the strict two-body quadrupoles included in the stresslet-free interactions differ dramatically from the proper many-body quadrupoles, which are somehow captured through the mean-field quadrupole in the Rotne–Prager approximation. It is known, for example (cf. Brady *et al.*[13]), that in periodic systems it is the many-body higher moments, not the two-body moments, that give the proper behavior at high ϕ. In any event, it is clear that the neglect of stresslet interactions is the key first step to understanding particle interactions in sedimenting suspensions. A thorough understanding of the effects of higher moments requires more study.

Now that we understand the nature of the Rotne–Prager approximation and why it works reasonably well, we can actually derive an analytical expression for the sedimentation rate. As mentioned in Sec. II, the first integral on the rhs of Eq. (10) vanishes in the Rotne–Prager approximation and the second integral can be calculated analytically if we use the Percus–Yevick radial distribution function. Using the Laplace transform of $rg(r)$ given by Mansoori *et al.*,[25] the sedimentation velocity is

$$\langle U \rangle - \langle u \rangle = 1 + \phi - \frac{1}{5}\phi^2 - \frac{6}{5}\phi\left(\frac{5 - \phi + \frac{1}{2}\phi^2}{1 + 2\phi}\right). \tag{16}$$

The analytical expression (16) is the dashed line in Fig. 2 and agrees very well with the calculations ($\times$'s) using the better expression for the hard-sphere $g(r)$. Equation (16) can be considered a correlation for sedimentation rate, but, unlike most correlations, it is based on an understanding of the hydrodynamic interactions in a sedimenting suspension.

A final point that also requires further comment is the sedimentation rate of disordered suspensions in the limit $\phi \to 0$. Batchelor's[2] result, $U/U_0 = 1 - 6.55\phi$, is based on the full pairwise two-sphere interaction, i.e., it includes all moments, including stresslets. Using the Rotne–Prager approximation [cf. Eq. (16)], the $\phi \to 0$ result is $U/U_0 = 1 - 5\phi$. From Fig. 3, it is not clear whether U_x^S for one sphere sedimenting through a suspension of neutrally buoyant spheres will differ from U_x^S for sedimenting systems in the limit $\phi_A \to 0$. The two results should converge, however, as $\phi_A \to 0$ (and as $\phi \to 0$) because the stresslet correlation length will increase as $\phi \to 0$. Batchelor's result should be recovered unless there is some additional ϕ-dependent length in the problem. Unfortunately, the dilute limit is difficult to study through simulation, as very small effects must be compared and issues of system size, the effect of periodic boundary conditions, etc., must be considered. Experimental results do not seem to give Batchelor's coefficient, generally giving a

value of less than 6.55. However, it should be realized that a volume fraction of $\phi = 0.05$ is not "small" as far as hydrodynamic interactions are concerned. This can be seen from Eq. (16), where at $\phi = 0.05$ the sedimentation velocity is predicted to be 0.78, as opposed to 0.75 if $1 - 5\phi$, the linear asymptotic form, is used. The discrepancy becomes even more pronounced at higher ϕ, giving a 20% error in the coefficient at $\phi = 0.1$. Thus extrapolations of the behavior as $\phi \to 0$ that include data from $\phi > 0.05$ may not give reliable estimates of the $O(\phi)$ coefficient.

V. CONCLUSIONS

In Secs. I–IV we have discussed the sedimentation rate of a hard-sphere suspension, the interactions between particles in such a system, and the "effective" behavior of both sedimenting and free suspensions. It was seen that spheres in sedimenting suspensions are essentially stresslet-free and that approximations for sphere interactions that capture this yield reasonable sedimentation velocities. Because spheres in sedimenting systems are stresslet-free, the "effective" behavior of these systems is quite different than that of free suspensions, which act as a fluid with an effective viscosity. Recent effective continuum approaches for predicting the sedimentation velocity[26] have used the notion of an effective viscosity and have recovered good estimates of the behavior as $\phi \to 0$. It is not clear how these approaches could be modified to incorporate the notion of stresslet-free interactions, which appears to be essential at higher ϕ.

We have also seen that the very simple Rotne–Prager approximation, which results in simple integration formulas that can be performed analytically for the Percus–Yevick hard-sphere distribution, gives reasonable estimates of sedimentation velocities. This same approach should apply to polydisperse suspensions; thus we have a simple means (and with the Percus–Yevick distribution functions for mixtures of particles of various sizes an analytical means) to predict the sedimentation rate of mixtures.[27]

Through simulation, we were able to investigate fundamental aspects of particle interactions in sedimenting systems and as a result elucidate the effective behavior of such systems. In a previous paper,[28] we applied Stokesian dynamics to the study of the effective behavior of porous media. It is our feeling that simulation, particularly when used in conjunction with theory, as in the present problem, will continue to find use in effective medium problems and help in our understanding of such systems.

ACKNOWLEDGMENTS

We wish to thank J. Lester for her assistance with several aspects of the computations.

Partial support for this work was through National Science Foundation Grant No. CBT-8696067. Computer time was supplied by the San Diego Supercomputer center.

APPENDIX: EFFECTIVE VISCOSITY OF FREE SUSPENSIONS

The purpose of this Appendix is to present a simple calculation to show that when one particle (more precisely a point force) is sedimenting through a suspension of neutrally buoyant particles, the suspension may be modeled as a homogeneous fluid with an effective viscosity $\eta_{\text{eff}} = (1 + \frac{5}{2}\phi)\eta$ in the dilute limit $\phi \to 0$. We make no claims to originality of this demonstration, as Beenakker and Mazur[10] have shown explicitly that Einstein's viscosity is recovered in the dilute limit [cf. Eq. (6.10) of Ref. 10]. The demonstration given here, however, may help make this result accessible to readers unfamiliar with Beenakker and Mazur's rather complex analysis and may aid in our understanding of suspension behavior.

The problem to be addressed is to find the form of the propagator, or Green's function, for a point force in a suspension of force- and torque-free particles. For a pure fluid, the Stokeslet or propagator is simply

$$(1/8\pi\eta)(\delta_{ij}/r + r_i r_j / r^3) \tag{A1}$$

and gives the ith component of the velocity at point $\mathbf{r}$ due to the jth component of a point force located at the origin. We shall show that the *form* of (A1) is unchanged by the presence of neutrally buoyant particles, but the amplitude is modified by replacing η by η_{eff}.

We can think of the propagator as "propagating" the disturbance from the force at the origin to the point $\mathbf{r}$. In a suspension, part of this disturbance will be scattered from other particles before arriving at the field point $\mathbf{r}$. It is the sum of all these scatterings that we wish to calculate. When a velocity disturbance is incident on a neutrally buoyant particle located at $\mathbf{x}_3$, it induces a stresslet in this particle of magnitude $O(1/r_{31}^2)$. Here, the subscript 31 indicates that we are evaluating the stresslet of the particle located at $\mathbf{x}_3$ due to a point force located at $\mathbf{x}_1$, $r_{31} = |\mathbf{x}_3 - \mathbf{x}_1|$. This particle "scatters" the incident velocity disturbance by propagating in turn a stresslet velocity disturbance that decays as $1/r_{23}^2$ times the stresslet intensity, resulting in a velocity disturbance of $O[1/(r_{23}^2 r_{31}^2)]$ at the point $\mathbf{x}_2$. Here, we have labeled the point $\mathbf{r}$ at which we measure the velocity disturbance $\mathbf{x}_2$, so that $\mathbf{r}$ becomes $\mathbf{r}_{21}$ in (A1).

Thus the effect of a particle is $O(1/r^4)$, which is both smaller than (A1) and of a different character, a fourth as opposed to first dependence on inverse distance. However, we must add up the contributions from *all* the "second" particles by multiplying by the probability for finding a particle at $\mathbf{x}_3$ given that there is one at the origin and integrating over all space. The probability density is approximately ϕ and after integration, the resultant integral of $1/(r_{23}^2 r_{31}^2)\phi\, dV_3$ is $O(\phi/r_{21})$. This has the same form as the Stokeslet (A1), decaying as one over distance, but with an $O(\phi)$ amplitude.

This is the scattering from the induced stresslet of just one "second" particle. Before being incident at the field point $\mathbf{x}_2$, however, the scattered velocity from 3 may strike a third particle at 4. The particle at 4 will have an induced stresslet of intensity $O[1/(r_{43}^3 r_{31}^2)]$, and we must now average over all particles 4 *and* over all particles 3, i.e., $\phi^2\, dV_3\, dV_4$. The resulting integration produces a correction of the form $O(\phi^2/r_{21})$, which has the *same r* dependence as the free-space or "bare" propagator (A1). The sequence should now be clear: A third particle located at 5 will con-

tribute $O(\phi^3/r_{21})$, or the nth particle will contribute $O(\phi^n/r_{21})$. An infinite series of the form $\Sigma_{n=0}\phi^n/r_{21}$ is formed and the sum of this series results precisely in Einstein's viscosity $[(1+\frac{5}{2}\phi)r_{21}]^{-1}$.

All of this discussion is for reflected stresslet interactions only and, as we shall see shortly, for homogeneous, random, structureless suspensions. Higher moments than stresslets are, of course, important, but they will enter only as terms of $O(1/r_{21}^2)$, etc., and thus are of a different nature than that of the effective viscosity. We shall not concern ourselves here with these higher order terms, as the point of the calculation is just to show that an effective viscosity in place of η in (A1) is meaningful for a point force in a suspension of neutrally buoyant particles.

To carry out the explicit demonstration, we need to introduce a bit of notation. We shall introduce the differential operator $\mathbf{q}$ that performs a symmetric derivative of an incident velocity field to obtain the stresslet and then propagates the stresslet velocity disturbance. With an incident velocity field $\mathbf{v}$, the scattered velocity field $\mathbf{u}$ is given by

$$u_i = q_{ij}v_j \equiv K_{ijk}\tfrac{1}{2}(\nabla_j v_k + \nabla_k v_j), \tag{A2}$$

where

$$K_{ijk} = \tfrac{20}{3}\pi a^3 \tfrac{1}{2}(\nabla_j J_{ik} + \nabla_k J_{ij}) \tag{A3}$$

and $\mathbf{J}$ is the point force propagator (A1) without the factor $1/\eta$, i.e., the same $\mathbf{J}$ defined in Eq. (2). We note that $\mathbf{K}$ is also related to the $\mathbf{K}$ of Eq. (3), except that in (A3) there is the factor $\frac{20}{3}\pi a^3$.

With this notation, we may write the following for the velocity field at 2 resulting from a point force at 1 and a contribution from a stresslet scatterer at 3:

$$\mathscr{J}_{ij}^{21} \approx J_{ij}^{21} + q_{ik}^{23}J_{kj}^{31}. \tag{A4}$$

Here, $\mathscr{J}_{ij}^{21}$ represents the "effective" propagator—that is, the propagator that includes the many-body scattering that we seek to calculate; J_{ij} is the "bare" propagator and q_{ik} gives the stresslet scattering. The superscripts give the sequence of scatterings: field at 2 resulting from force at 1, etc.

We must now add up all particles at 3 by multiplying by $P_{1/2}(\mathbf{x}_3|\mathbf{x}_1,\mathbf{x}_2)$, the conditional probability density for finding a particle at $\mathbf{x}_3$ given that there is a particle at $\mathbf{x}_1$ (the source point) and *no* particle at $\mathbf{x}_2$ (the field point). We could, of course, actually have a particle at $\mathbf{x}_2$; then (A4) would give the first approximation to the velocity of the particle at $\mathbf{x}_2$. Since $P_{1/2} \approx n$, the number density of particles, we may thus write

$$\mathscr{J}_{ij}^{21} \approx J_{ij}^{21} + n\int q_{ik}^{23}J_{kj}^{31}\,dV_3 + \int [P_{1/2}(\mathbf{x}_3|\mathbf{x}_1,\mathbf{x}_2) - n]q_{ik}^{23}J_{kj}^{31}\,dV_3. \tag{A5}$$

The second integral on the rhs of (A5) will be $o(1/r_{21})$ and therefore we shall neglect it, as it is a different order in $1/r$. In essence, we are assuming the particles can overlap each other freely, that is, they are penetrable spheres, for which n is the correct value for $P_{1/2}$.

We continue in this way, adding the two-body scattering term

$$\int P_{2/2}(\mathbf{x}_3,\mathbf{x}_4|\mathbf{x}_1,\mathbf{x}_2)q_{il}^{24}q_{lk}^{43}J_{kj}^{31}\,dV_3\,dV_4, \tag{A6}$$

as well as the equivalent term with 3 and 4 interchanged, and assuming $P_{2/2} \sim n^2$, etc., to obtain

$$\mathscr{J}_{ij}^{21} \approx J_{ij}^{21} + n\int q_{ik}^{23}J_{kj}^{31}\,dV_3 + 2n^2\int q_{il}^{24}q_{lk}^{43}J_{kj}^{31}\,dV_3\,dV_4 + \cdots. \tag{A7}$$

The order of scatterings is taken to be unique in (A7), where all possible combinations of scatterings from 2, 3, 4, etc., pairs of particles that when integrated will give a contribution of $O(1/r_{21})$ are considered, i.e., each particle only scatters once.

Solution of (A7) for $\mathscr{J}_{ij}^{21}$ can be obtained by Fourier transformation and repeated use of the convolution theorem. It is in this step that we require the approximation that $P_{m/2} = n^m$ for a group of m particles, i.e., that there is no structure in the suspension. As remarked earlier, this approximation is simply a detail and the neglected terms in the final expression for $\mathscr{J}_{ij}$ are $o(1/r_{21})$ and thus are of lower order than those retained here. Denoting the Fourier transform by a caret, (A7) becomes

$$\hat{\mathscr{J}}_{ij} = \hat{J}_{ij} + n\hat{q}_{ik}\hat{J}_{kj} + 2n^2\hat{q}_{il}\hat{q}_{lk}\hat{J}_{jk} + \cdots. \tag{A8}$$

Note that there are no longer any labels on the sequence of $\mathbf{q}$'s and $\mathbf{J}$'s as the convolution theorem has removed them. We also see from (A8) the inherent linearity of the sequence of scatterings, as all terms are proportional to the original source $\mathbf{J}$.

To make further progress, we must examine the precise forms of $\hat{\mathbf{J}}$ and $\hat{\mathbf{q}}$. From (A2) and (A3), we see that

$$n\hat{q}_{ik}\hat{J}_{kj} = -\phi(\tfrac{5}{4})(k_k\hat{J}_{il} + k_l\hat{J}_{ik})(k_k\hat{J}_{lj} + k_l\hat{J}_{kj}) \tag{A9a}$$

$$= -\tfrac{5}{2}\phi k^2[\hat{J}_{ik}\hat{J}_{kj} + \tfrac{1}{2}\hat{k}_k\hat{k}_l(\hat{J}_{il}\hat{J}_{kj} + \hat{J}_{ik}\hat{J}_{lj})], \tag{A9b}$$

where $\mathbf{k}$ is the transform variable corresponding to $\mathbf{r}$ and $\hat{\mathbf{k}} = \mathbf{k}/k$.

The next term in (A8) is

$$2n^2\hat{q}_{il}\hat{q}_{lk}\hat{J}_{kj} = 2\phi^2(\tfrac{5}{4})^2(k_n\hat{J}_{il} + k_l\hat{J}_{in}) \times [k_n(k_k\hat{J}_{lm} + k_m\hat{J}_{lk})(k_k\hat{J}_{mj} + k_m\hat{J}_{kj}) + k_l(k_k\hat{J}_{nm} + k_m\hat{J}_{nk})(k_k\hat{J}_{mj} + k_m\hat{J}_{kj})] \tag{A10a}$$

$$= (\tfrac{5}{2}\phi)^2k^4[\hat{J}_{il}\hat{J}_{lm}\hat{J}_{mj} + \tfrac{1}{2}\hat{k}_k\hat{k}_m\hat{J}_{il}\hat{J}_{lm}\hat{J}_{kj} + \cdots]. \tag{A10b}$$

Now, we note that the Fourier transform of J_{ij} is

$$\hat{J}_{ij} = (\delta_{ij} - \hat{k}_i\hat{k}_j)/k^2 = a(k)(\delta_{ij} - \hat{k}_i\hat{k}_j). \tag{A11}$$

Substituting (A11) into (A9b), (A9b) becomes

$$n\hat{q}_{ik}\hat{J}_{kj} = -\tfrac{5}{2}\phi k^2 a(k)a(k)(\delta_{ij} - \hat{k}_i\hat{k}_j). \tag{A9b'}$$

Similary, (A10b) becomes

$$2n^2\hat{q}_{il}\hat{q}_{lk}\hat{J}_{kj} = +[\tfrac{5}{2}\phi k^2 a(k)]^2 a(k)(\delta_{ij} - \hat{k}_i\hat{k}_j). \tag{A10b'}$$

The sequence of terms continues with alternating signs from the $(-i)^{2n}$ factor from the derivatives in $\mathbf{q}$ and each term

has a factor of $[-\frac{5}{2}\phi k^2 a(k)]^n$ times $a(k)(\delta_{ij}-\hat{k}_i\hat{k}_j)$. However, $k^2 a(k)=1$, so the sequence becomes

$$\hat{\mathscr{J}}_{ij}=\sum_{n=0}^{\infty}\left(-\frac{5}{2}\phi\right)^n a(k)(\delta_{ij}-\hat{k}_i\hat{k}_j), \tag{A12}$$

or

$$\hat{\mathscr{J}}_{ij}=\frac{1}{1+\frac{5}{2}\phi}\frac{\delta_{ij}-\hat{k}_i\hat{k}_j}{k^2}=\frac{1}{1+\frac{5}{2}\phi}\hat{J}_{ij}. \tag{A13}$$

Hence, the effective or "renormalized" propagator is just the "bare" propagator, with the fluid viscosity replaced by Einstein's viscosity.

This procedure can be generalized to include scatterings from all higher moments by defining $\mathbf{q}$ to contain the quadrupole, octupole, etc., moments, and then by including scattering sequences where the same particle can participate more than once. With the general sequence written down, the Fourier transform and convolution theorem can again be used for a homogeneous, isotropic, structureless suspension; this will reproduce precisely the "renormalized connectors" of Beenakker and Mazur,[10] specifically, their Eq. (6.9): The low k, or large r expansion of their expression is the formula (A13) computed here.

[1]R. H. Davis and A. Acrivos, Annu. Rev. Fluid Mech. **20**, 91 (1985).
[2]G. K. Batchelor, J. Fluid Mech. **52**, 245 (1972).
[3]H. Hasimoto, J. Fluid Mech. **5**, 317 (1959).
[4]P. G. Saffman, Stud. Appl. Math. **52**, 115 (1973).
[5]A. S. Sangani and A. Acrivos, Int. J. Multiphase Flow **8**, 343 (1982).
[6]A. Zick and G. M. Homsy, J. Fluid Mech. **115**, 13 (1982).
[7]A. B. Glendinning and W. B. Russel, J. Colloid Interface Sci. **89**, 124 (1982).
[8]R. W. O'Brien, J. Fluid Mech. **91**, 17 (1979).
[9]L. A. Mondy, A. L. Graham, and J. L. Jensen, J. Rheol. **30**, 1031 (1986).
[10]C. W. J. Beenakker and P. Mazur, Physica **120A**, 388 (1983).
[11]J. F. Brady and G. Bossis, Annu. Rev. Fluid Mech. **20**, 111 (1988).
[12]L. Durlofsky, J. F. Brady, and G. Bossis, J. Fluid Mech. **180**, 21 (1987).
[13]J. F. Brady, R. J. Phillips, J. C. Lester, and G. Bossis, J. Fluid Mech. (in press).
[14]M. S. Wertheim, Phys. Rev. Lett. **10**, 321 (1963).
[15]E. Thiele, J. Chem. Phys. **39**, 474 (1963).
[16]G. J. Throop and R. J. Bearman, J. Chem. Phys. **42**, 2408 (1965).
[17]W. R. Smith and D. Henderson, Mol. Phys. **19**, 411 (1970).
[18]J. A. Barker and D. Henderson, Mol. Phys. **21**, 187 (1971).
[19]L. Verlet and J. J. Weis, Phys. Rev. A **5**, 939 (1972).
[20]P. Perry and G. J. Throop, J. Chem. Phys. **57**, 1827 (1972).
[21]D. J. Jeffrey and Y. Onishi, J. Fluid Mech. **139**, 261 (1984).
[22]J. Garside and M. R. Al-Dibouni, Ind. Eng. Chem. Process Des. Develop **16**, 206 (1977).
[23]D. G. Chae, F. M. Ree, and T. Ree, J. Chem. Phys. **50**, 1581 (1969).
[24]S. Kim and R. T. Mifflin, Phys. Fluids **28**, 2033 (1985).
[25]G. A. Mansoori, J. A. Provine, and F. B. Canfield, J. Chem. Phys. **51**, 5292 (1969).
[26]A. Acrivos and E. Y. Chang, in *Physics and Chemistry of Porous Media II*, edited by J. R. Banavar, J. Koplik, and K. W. Winkler, AIP Conference Proceedings 154 (American Institute of Physics, New York, 1987), p. 27.
[27]J. F. Brady (to be submitted).
[28]L. Durlofsky and J. F. Brady, Phys. Fluids **30**, 3329 (1987).